Energy & Environmental Science

Cite this: DOI: 10.1039/c2ee21376a

www.rsc.org/ees

PAPER

Modeling geminate pair dissociation in organic solar cells: high power conversion efficiencies achieved with moderate optical bandgaps†

Jonathan D. Servaites,[ac] Brett M. Savoie,[bc] Joseph B. Brink,[cd] Tobin J. Marks*[abc] and Mark A. Ratner*[abc]

Received 14th February 2012, Accepted 1st May 2012
DOI: 10.1039/c2ee21376a

We propose a model for geminate electron–hole dissociation in organic photovoltaic (OPV) cells and show how power conversion efficiencies greater than those currently achieved might be realized *via* design strategies employing moderate optical bandgaps and enhanced charge delocalization near the donor–acceptor interface. Applying this model to describing geminate electron–hole dissociation *via* charge transfer (CT) states, we find good agreement with recently published high-efficiency experimental data. The optimal bandgap for current-generation organic active layer materials is argued to be ~1.7 eV – significantly greater than in previous analyses, including the Shockley–Queisser approach based upon non-excitonic solar cell dynamics. For future higher efficiency OPVs, the present results show that the optimal bandgap should be slightly lower, ~1.6 eV. Finally, these results support design strategies aimed at enhancing mobility near the donor–acceptor interface and reducing the electron–hole binding energy, rather than striving to further reduce the bandgap.

1. Introduction

Organic photovoltaic (OPV)[1] cells[1–12] offer a promising approach to solar energy conversion due to low materials and manufacturing costs, use of earth-abundant materials, mechanical flexibility, and versatile chemical design.[6,8,13] Recent bulk heterojunction (BHJ) OPV advances have provided power conversion efficiencies (PCEs) >8%,[7,9,14] with media reports stating over 9% (ref. 15 and 16) for single layer cells and over 10% for tandem cells.[17] Nevertheless, further performance advances are critical for large-scale OPV deployment, and achieving such advances presents a fundamental scientific challenge.

While state-of-the-art OPVs (Fig. 1a) typically have lower PCEs than their inorganic counterparts,[14] they exhibit several attractive performance characteristics. Fill factors for many designs are high (≥70%),[10,18] as are optical absorption (~90%) and internal quantum efficiencies (near 100%), indicating that under short circuit conditions, exciton diffusion, electron–hole

[a]*Department of Materials Science and Engineering, 2145 Sheridan Road, Evanston, IL 60208, USA*
[b]*Department of Chemistry, Northwestern University, 2145 Sheridan Road, Evanston, IL 60208, USA. E-mail: ratner@northwestern.edu; t-marks@northwestern.edu; Tel: +1-847-491-5652*
[c]*Argonne-Northwestern Solar Energy Research Center, 2145 Sheridan Road, Evanston, IL 60208, USA. E-mail: ANSER@Northwestern.edu; Fax: +1-847-467-1425; Tel: +1-847-467-4910*
[d]*School of Engineering & Applied Science, Yale University, 10 Hillhouse Avenue, New Haven, CT 06511, USA*
† Electronic supplementary information (ESI) available. See DOI: 10.1039/c2ee21376a

Broader context

The planet's solar energy resources are vast: more energy from the sun hits the Earth in one hour than all of humankind consumes over an entire year. However, due largely to high costs, solar cells comprise far less than 1% of the world's energy mix. While some cost reductions will be achieved through economies of scale, new solar cell materials and architectures are needed for large cost reductions. Organic solar cells offer potential routes to large-scale solar deployment based on the possibility of large cost reductions using earth-abundant materials and inexpensive production technologies. Nevertheless, despite recent advances in performance, organic solar cell efficiencies lag behind their inorganic counterparts, and new materials are needed to enhance performance. Furthermore, existing performance limitations are not completely understood and are one reason for organic solar cells not yet reaching their full potential. In this Paper, we propose a model for geminate pair recombination, which is regarded as a key loss mechanism in organic solar cells. Through application of the model, we suggest strategies for achieving high power conversion efficiencies.

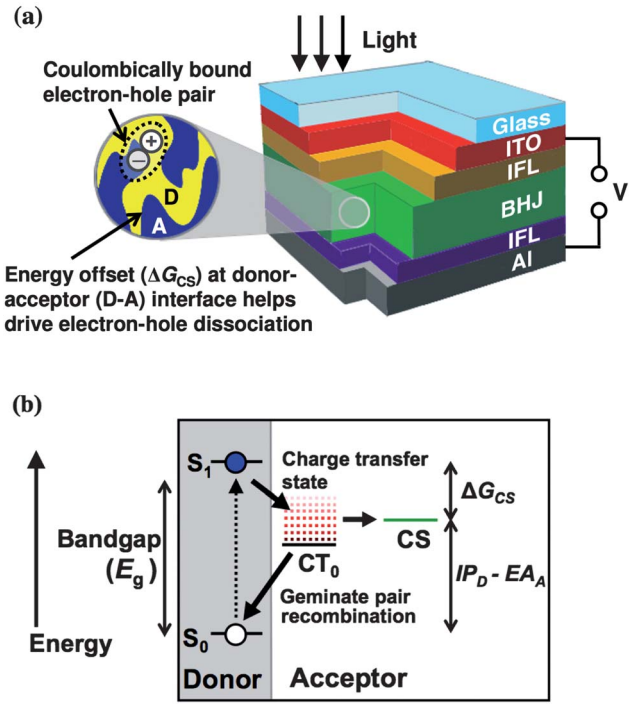

Fig. 1 Donor–acceptor energy offsets (ΔG_{CS}) and organic solar cell performance. (a) A bulk-heterojunction (BHJ) organic solar cell showing the Coulombically bound geminate electron–hole pair. Energy offsets at the interface of the donor (yellow) and acceptor (blue) materials drive electron–hole dissociation. ITO = indium tin oxide (a transparent electrode), IFL = interfacial layer, BHJ = bulk-heterojunction absorber layer, and Al = aluminum. (b) Energy landscape at the donor–acceptor interface in an organic solar cell (based on ref. 11). S_0 is the singlet ground state, S_1 is the singlet excited state, and CT_0 is the lowest energy singlet charge transfer state. The dotted red lines represent the multiple higher energy CT vibronic states. We define the energy offset ΔG_{CS} as $\Delta G_{CS} = E_{g,D} - (IP_D - EA_A)$, where IP_D is the ionization potential of the donor and EA_A is the electron affinity of the acceptor. ΔG_{CS} here represents the lower limit to the thermal energy available for dissociation. Note that triplet states[38–40] are not shown. The donor and acceptor labels indicate the location of the electron. Note that "geminate pair dissociation" from a CT state to the charge separated state is the focus of the model here.

dissociation, and charge collection efficiencies can approach 100%.[10,19] A critical remaining challenge in OPV design is realizing high performance materials having minimal donor–acceptor energy offsets, ΔG_{CS} (Fig. 1b).[8,20–22] Such offsets act at the donor–acceptor interface to drive exciton dissociation (Fig. 1a and b), however they also create parasitic energy losses and can greatly limit PCE.[8,20–22] For example, with ΔG_{CS} = 1.0 eV, OPVs are unlikely to exceed 6% power conversion efficiency even with complete exciton dissociation, because of the large energy loss.[22] It is therefore imperative to design OPV materials with high dissociation efficiencies at low energy offsets. Well-optimized organic solar cells with low offsets ($\Delta G_{CS} \approx$ 0.2–0.3 eV)[23,24] typically exhibit lower power conversion efficiencies than their high offset counterparts ($\Delta G_{CS} \approx$ 0.5–0.7 eV) (ref. 7 and 9)‡ despite the benefit of reduced voltage losses at low offsets.[20,25] Previous studies have reported progress in reducing ΔG_{CS} while increasing PCE;[26] however, there remains the need for further ΔG_{CS} reduction and the development of models and theoretical frameworks to account for incomplete exciton dissociation with respect to ΔG_{CS} and other OPV properties.

Previous models of exciton dissociation have largely employed Braun's adaptation of Onsager's geminate dissociation theory (OB theory).[27–32] While OB theory can fit OPV current–voltage data, these models require assumptions about mobility or charge transfer (CT, Fig. 1b) state lifetimes§ that are inconsistent with experiment.[33–36] Furthermore, OB does not directly quantify donor–acceptor energy offset effects,[31,37] limiting its utility for materials design. Importantly, the physical assumptions of OB – full thermalization of an intermediate species followed by a diffusive walk – cannot be reconciled with the ultrafast timescales consistently reported for dissociation.[35,36] The observation of such short timescales has led to a lively discussion in the literature about the possible role of "hot states," (Fig. 1b) *i.e.*, short-lived vibrationally excited states, in mediating exciton dissociation.[41–45] Our motivation here is to present a model for vibrationally assisted "hot dissociation" that will help ascertain the limits of such a mechanism for describing exciton dissociation (more specifically, "geminate pair dissociation") and its implications for device performance.

To model the hot dissociation process, we have adapted a description of carrier photogeneration in pristine materials by Arkhipov *et al.*[46] The proposed dissociation process is: following electron transfer from donor to the acceptor, a hot CT state is created with excess energy ΔG_{CS} populating local vibrational modes.[42,45,47–49] While available, this excess energy can thermally promote dissociation of the Coulombically bound electron–hole pair (Fig. 1b). Charge dissociation then occurs in competition with the decay of this excess energy (with first order rate constant β; Fig. 1b). In light of the ultrafast timescales ascribed to exciton dissociation by recent spectroscopic studies, it is considered unlikely that the excess energy ΔG_{CS} has fully dissipated from the CT species. This renders the CT state "hot," by which we mean that the energy ΔG_{CS} resides in local vibrational modes (Fig. 1b), in agreement with the suggestion of Pensack and Asbury.[41]

In accordance with recent ultrafast transient spectroscopy studies, the proposed model also suggests that charge generation should be limited to a timescale of the same order of magnitude as vibrational frequencies, and that fully relaxed CT states represent a loss channel.[36,50,51] The states in this charge transfer and dissociation process are shown in Fig. 1b.[11,38,42,52,53] (Fig. 1b is adapted from ref. 11).

To explore the limits of this dissociation mechanism in explaining trends in the field, we incorporate the generation equations into a simple device model that permits calculation of PCE. This approach provides a means of relating ΔG_{CS} to the PCE of devices. Comparison of experimental data sets of PCE *vs.* ΔG_{CS} is used to ascertain the limits of hot dissociation as a predictive dissociation mechanism. The results of this analysis suggest that a moderate bandgap = ~1.65 to 1.7 eV is optimal for

‡ We focus here on the dissociation of excitons originating on the donor. As alternative acceptor materials are developed that absorb more light, analogous considerations must be made for acceptor side dynamics.

§ Note that mathematically the effect of mobility and CT lifetime on exciton dissociation are identical and cannot be distinguished by OB theory.

the current generation of OPVs, in accord with the recent empirical observations of Nayak *et al.*[54] We also present calculations for ΔG_{CS} *vs.* PCE, quantifying how low ΔG_{CS} magnitudes may depress PCEs below values based on ideal dissociation.

2. Methodology

2.1 Modeling geminate pair dissociation efficiency (η_{diss})

The model developed by Arkhipov *et al.* suggests that excess energy ($h\nu - E_g$) from an above bandgap excitation remains in local vibrations long enough to thermally assist dissociation of the exciton.[46] The model predicts that geminate pair dissociation is a competition between the thermal dissociation rate and the decay of the excess energy; once the excess energy is expended, dissociation is considered improbable.

Key physical assumptions in the derivation of Arkhipov *et al.* include definitions for the geminate pair dissociation barrier and the rate of dissociation. In the model, the potential energy of the CT species is described as a superposition of the Coulombic attraction with the external electric field. This introduces a mechanism for the external field to lower the energetic barrier for geminate pair dissociation. The model also assumes a thermally assisted mechanism and a Boltzmann rate of dissociation. Physically, this implies that dissociation occurs on a timescale long enough for a local thermal distribution to be reached. This physical picture can be extended to geminate pair dissociation at a donor–acceptor interface by equating the ΔG_{CS} supplied by the energy offset between the exciton (S_1) and charge-separated states (CS), with $h\nu - E_g$ in the original paper.[46] The probability of geminate pair dissociation then becomes:

$$p_d = 1 - \exp\left[-\frac{\nu_0}{\beta}\int_{kT}^{\langle E_{cs}\rangle + kT} dE_{phon} \exp\left(\frac{-E_{GP}}{E_{phon}} + \frac{e}{E_{phon}}\sqrt{\frac{eFz}{\pi\varepsilon_0\varepsilon_r}}\right)\right] \quad (1)$$

where ν_0 is the attempt-to-jump frequency from charge transfer to charge separated states (referred to hereafter as the "jump frequency"), β the first-order decay constant of excess thermal energy, k the Boltzmann constant, E_{phon} the local phonon energy available for dissociation, e the elementary charge, E_{GP} the geminate pair binding energy (*i.e.*, the binding energy in the CT state), F the electric field strength, z the cosine of the angle between the electric field and the dissociation direction, ε_0 the permittivity of free space, and ε_r the dielectric constant. Note that the upper limit to the second exponential is set at unity.[46] The integral limits $kT + \langle E_{CS}\rangle$, and kT represent the points at which all the excess energy is available to aid dissociation and at which all the excess energy is fully dissipated, respectively. $\langle E_{CS}\rangle$ is the initial excess bath energy given by eqn (2)

$$\langle E_{CS}\rangle = \alpha \Delta G_{CS} \quad (2)$$

where α is a unitless constant related to the local heat capacity (C) by $\alpha = k/C$, and ΔG_{CS} is defined as:

$$\Delta G_{CS} = E_{g,D} - (IP_D - EA_A) \quad (3)$$

where $E_{g,D}$ is the donor bandgap, IP_D ionization potential of the donor material, and EA_A is the electron affinity of the acceptor. It should be noted that ΔG_{CS} represents the lower limit to the thermal energy available for dissociation following electron transfer. The lowest CT state of a given system may in fact be lower in energy and is expected to vary from system to system.[25]

The overall dissociation probability is then averaged by integrating eqn (1) over all orientations with the electric field, where $p_d(z)$ is the dissociation probability for a given angle θ and $z = \cos\theta$:

$$\eta_{diss} = \frac{2}{\pi}\int_0^1 p_d(z)dz \quad (4)$$

Eqn (4) is evaluated using the experimentally deduced values of $\varepsilon_r = 3.5$, $\nu_0 = 40$ ps^{-1}, and $\beta = 0.3$ eV ps^{-1},[46,55,56] all of which are representative of OPV materials. Note that β represents the rate of thermal decay away from the CT species to the greater system (considered here to be the bath). This intermolecular dissipation is expected to be slower than the intramolecular thermalization that occurs upon electron transfer. The value for β has been selected to be consistent with thermal conductivities for conducting polymers.[46,57] α and E_{GP} are fit to PTB7:$PC_{71}BM$ device data (Fig. 2) to reproduce the short circuit current and are calculated to be 0.043 and 100 meV, respectively. These values also are comparable to literature values, where $\alpha = \sim 0.03$ to 0.06 (ref. 46 and 58) and $E_{GP} = 0.13$ eV.[59] The electric field is

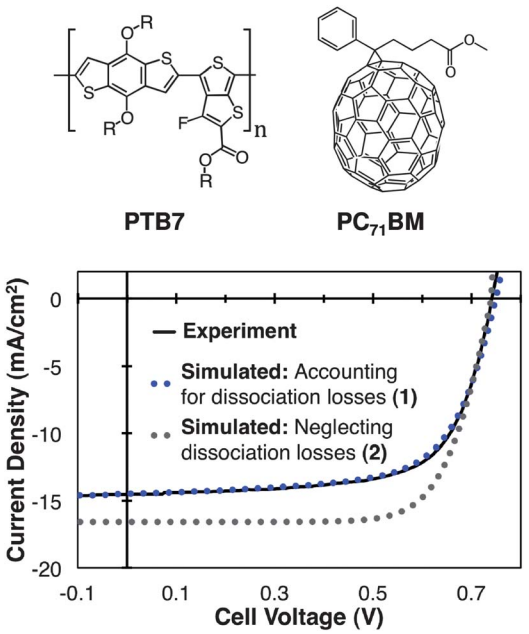

Fig. 2 Influence of charge dissociation efficiency on OPV performance. Experimental *JV* data from a current state-of-the-art organic solar cell *vs.* two simulated cases. The experimental data[9] are from a cell based on a PTB7:$PC_{71}BM$ donor–acceptor active layer, with a measured PCE = 7.4%.[9,69] As shown, $PC_{71}BM$ = phenyl-C_{71}-butyric acid methyl ester, and PTB7 is from the PTBX family of thieno[3,4-*b*]thiophene–benzodithiophene copolymers. Case 1: analysis of geminate pair dissociation taking $E_{GP} = 100$ meV and assuming geminate pair dissociation efficiency = 100% and $\Delta = 0.4$ V. Case 2 assumes complete dissociation. Assuming complete dissociation as long as $\Delta G_{CS} > 0.3$ eV (ref. 20 and 22) can lead to deviations between observed and projected performance (*e.g.*, compare the cases in Fig. 3).

$F = (V_0 - V)/d$, where V_0 is the built-in potential, V is the cell voltage, and d is active layer thickness.[20,29] We take $d = 100$ nm, which is representative of high performance OPVs.[7,9] For the baseline PTB7:$PC_{71}BM$ calculations, $E_{g,D}$ and IP_D assume experimental values of 1.73 eV and 5.15 eV, respectively. For determining experimental bandgaps from the literature, we use the midpoint of the absorption onset in the optical spectrum. In all calculations, the acceptor is taken to be $PC_{71}BM$ with an EA_A of −4.0 eV.[60] Note that, as was recently pointed out by Cardona *et al.*, discrepancies in the literature associated with determination of the frontier orbital energies have led to confusion in some studies employing these values.[61] Various techniques can yield different IP and EA energies, and it is therefore imperative to be consistent when determining ΔG_{CS} values.

At this level of analysis, we pragmatically neglect losses incurred by competitive energy transfer when the bandgap of the donor becomes too narrow, and geminate recombination to the triplet state. In the present discussion we focus on phonon-(vibrationally) assisted dissociation as the mechanism for geminate pair dissociation and do not explicitly treat the possibility of direct electron transfer to the charge separated state (*i.e.*, $S_1 \rightarrow$ CS). However, since eqn (4) is fit to experimental data for net current generation, dissociation by direct electron transfer or other mechanisms can contribute to the fit value of E_{GP}. Given the discussion in the literature about the role of hot dissociation,[41–45] our goal is to focus on the extent to which this mechanism alone can explain the experimental evidence. It should also be emphasized that this dissociation mechanism is not strictly dependent on excitation first to the S_1 state, followed by electron transfer; direct excitation of the CT state, where $\hbar\omega > E_{CT}$,¶ as in the studies of Drori *et al.*[44] and Lee *et al.*,[43] can still yield a "hot" state capable of complete or fractional dissociation.

Finally, it is expected that in specific systems the dissociation process will be influenced by the possible presence of multiple CT states and the specific electronic coupling of these states with the charge separated state. The model adopted here makes no assumptions about the actual nature of these states since the details of the interface are expected to be highly system dependent and our goal is to identify trends across systems. The model assumes a single intermediate state, an activation barrier, and an effective decay rate of excess energy. Within the context of this model, the presence of multiple electronic states at the interface as has been suggested by Muntwiler *et al.*[49] and recently by Bakulin *et al.*[62] would be expected to reduce the apparent rate of decay because of the generally longer lifetime of electronic excitations.

2.2 Modeling current–voltage curves and cell efficiency

The net solar cell current under operation is decomposed into dark and illuminated contributions according to eqn (5),

$$J(V) = J_{dark}(V) - J_{ph}(V) \quad (5)$$

The photocurrent J_{ph} can be expressed in terms of the bulk exciton generation rate (G) and geminate pair dissociation efficiency (η_{diss}),

$$J_{ph}(V) = eG\eta_{diss}(V) \quad (6)$$

$$G = \int \Phi_{AM1.5G}(\lambda)\eta_{trans}(\lambda)\eta_{abs}(\lambda)d\lambda \quad (7)$$

Here $\Phi_{AM1.5G}$ is the AM1.5G spectrum in photons s^{-1} nm^{-1} m^{-2}, η_{trans} is the optical transmission efficiency through the front electrode window, and η_{abs} is the wavelength dependent absorption efficiency. For $\eta_{trans}(\lambda)$, the previously reported transmission spectrum through ITO/glass is used (ITO = indium tin oxide).[22] Based on published state-of-the-art results, the absorption efficiency of above bandgap photons ($h\nu > E_g$) is taken as $\eta_{abs} = 90\%$,[22] and all excitons are assumed to reach an interface before recombination.[7,9,19] This assumption is a reasonable approximation based upon literature values in high performing OPVs.[19]

The *dark* current, J_{dark}, is modeled using the modified Shockley equation,

$$J_{dark}(V) = J_0\left(\exp\left(\frac{eV}{nk_BT}\right) - 1\right) + \frac{V - JR_s}{R_{sh}} \quad (8)$$

where R_s is the series resistance, R_{sh} is the shunt resistance, n is the diode ideality factor, and J_0 is the reverse saturation current. In all calculations $R_s = 2.5\ \Omega\ cm^2$ and $n = 1.8$; these values are taken as representative of well optimized devices.[11,22,63,64] Shunt resistance (R_{sh}) is taken to be near ideal (*i.e.*, $R_{sh} = 10^6\ \Omega\ cm^2$), which is consistent with optimized experimental cells.[10,65] As shown in the ESI (Fig. SI2†), an apparently low shunt resistance can appear under illumination while being absent from the dark curve. Within the context of our model this is the result of the field dependence of charge generation rather than the traditional diode shunt effect. J_0 remains the only undetermined variable required for evaluation of eqn (7). The value used for J_0 ultimately determines the V_{oc} of the device and in this model accounts for the non-geminate recombination processes[66] occurring in the cell. Previous work has suggested an empirical relationship for V_{oc} for devices with ohmic contacts:[20]

$$V_{oc} = \frac{1}{e}(EA_A - IP_D) - \Delta \quad (9)$$

Work by Vandewal *et al.*,[25] Veldman *et al.*,[67] and Giebink *et al.*[30] report similar relationships, where $\Delta = 0.3$ V is representative of well optimized devices. The physical interpretation of Δ remains debated. It has been variously interpreted as the binding energy of the CT state[25] and the disorder induced tail[54] in the density of states. We adopt it here only as an empirical factor.

Finally, eqn (8) can be substituted into eqn (5), the current set to zero, and J_0 solved for in terms of V_{oc} and the photocurrent,

$$J_0 = J_{ph}V_{oc}\left(\exp\left(\frac{eV_{oc}}{nk_BT}\right) - 1\right)^{-1} \quad (10)$$

In this treatment, bimolecular losses are treated empirically *via* eqn (9) and (10). As has been documented, these losses can vary substantially between systems, primarily being manifested in variations of fill factor and V_{oc}.[66,68] The approach taken here is adopted to focus on the role of exciton dissociation as a determinant for performance by holding all else equal, and is justified by the focus in this study on the limiting behavior of optimized systems.

Eqn (3)–(10) can be solved for a given system with information about the donor bandgap ($E_{g,D}$), the donor ionization potential

¶ E_{CT} is defined by the "cross-gap" minus the binding energy of the CT state, $E_{CT} = IP_D - EA_A - E_{GP}$.

(IP_D), and the acceptor electron affinity (EA_A), to generate a JV curve from which a power conversion efficiency can be calculated from the maximum power point (V_{max}, J_{max}) as, PCE = $J_{max}V_{max}/P_{in}$, where P_{in} is the total incident power of the AM1.5G spectrum. As described above, values for α and E_{GP} should be chosen to reproduce the experimental short circuit currents of a given system, and the value of Δ to reproduce the V_{oc}.

3. Results and discussion

3.1 Baseline: reproduction of state-of-the-art OPV materials

We use the well characterized PTB7:$PC_{71}BM$ system to establish a baseline case and demonstrate that the proposed methodology reproduces experiment.[9,69] For the geminate pair binding energy (E_{GP}), we calculate E_{GP} = 100 meV (accuracy at two significant figures) by fitting eqn (1) to reported high-efficiency OPV performance data,[9] based on a PTB7:$PC_{71}BM$ active layer (Fig. 2). Reported power conversion efficiencies for this system are between 7 and 8%.[9,69] The potential importance of accounting for geminate electron–hole pair dissociation dynamics is highlighted in Fig. 2 where there is good agreement with experiment when dissociation losses are accounted for, whereas significant deviations are noted when complete dissociation is assumed. Note that this approach assumes that charge dissociation is a limiting factor.

3.2 Organic solar cell efficiency limits

Using the value for E_{GP} obtained from the baseline calculation, Fig. 3 shows the ΔG_{CS} *vs.* PCE results derived from the model proposed here. ΔG_{CS} is varied in the calculations by changing the values of $E_{g,D}$ and IP_D, which corresponds physically to varying the energetics of the donor while keeping the acceptor, $PC_{71}BM$, constant. In the curve shown in Fig. 3 the donor bandgap is optimized for each ΔG_{CS}.

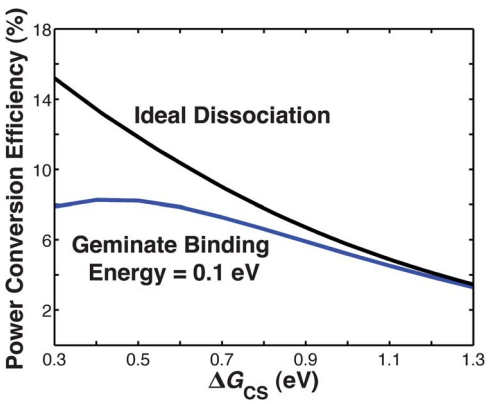

Fig. 3 Influence of geminate pair binding energy in limiting charge dissociation and power conversion efficiency. Calculated power conversion efficiencies based upon ideal (complete) dissociation and limited dissociation for the case of geminate pair binding energy = 100 meV, based upon the model proposed here. The greater deviation at lower ΔG_{CS} values between the two cases is due to suppressed charge dissociation efficiencies.

Fig. 3 shows two cases: the baseline cases (geminate pair binding energy = 100 meV) and the ideal dissociation case (*i.e.* complete dissociation or zero binding energy). Note that the two curves track each other well for large ΔG_{CS} values (~1.0 eV), but diverge markedly at lower ΔG_{CS} values. This reflects the suppression of charge dissociation efficiency at lower ΔG_{CS} values as predicted by eqn (1), when all other materials properties are held constant. Literature values for record OPV power conversion efficiencies tend to track the curve for 100 meV geminate pair binding energy case, especially for the higher ΔG_{CS} values.[7,9,70] Also, the highest efficiencies on this curve (~8%) are in line with recent media reports. The curves in Fig. 3 have been optimized for values of $E_{g,D}$ and IP_D. The effect of varying IP_D while holding ΔG_{CS} constant is included in the ESI (Fig. SI3†).

Fig. 4 shows calculated power conversion efficiencies based on ΔG_{CS} and $E_{g,D}$ values. Note that the energy level-PCE map differs substantially between the two cases (E_{GP} = 100 meV *vs.* the ideal case of no geminate pair binding energy, all other assumptions held constant). Thus, Fig. 4b presents the *ideal* scenario of complete geminate pair dissociation, while Fig. 4a describes the baseline case taken to be representative of current state-of-the-art systems. Fig. 4a suggests that 8–9% power conversion efficiencies are achievable for our chosen baseline cell properties, in line with current record OPV efficiencies.

Taken together, Fig. 3 and 4a predict that in general the optimal energy offset will be greater than the geminate pair binding energy,

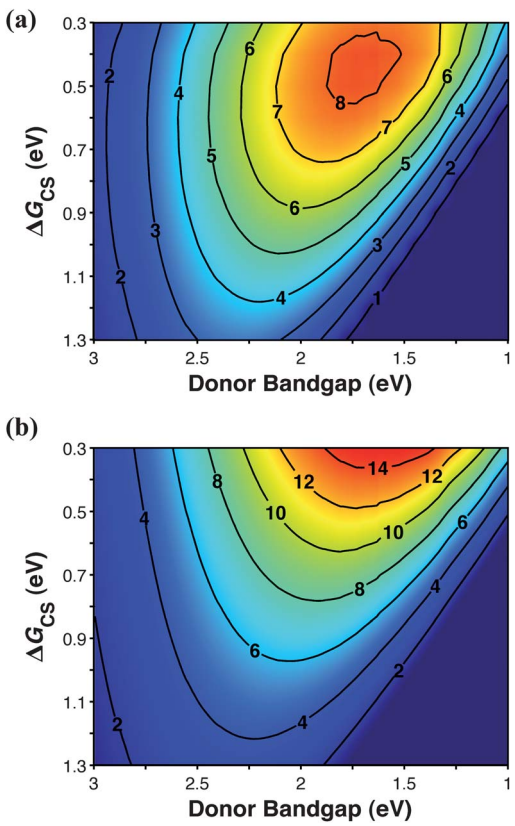

Fig. 4 Calculated OPV power conversion efficiencies as a function of donor bandgap and ΔG_{CS}. (a) Baseline case for geminate pair binding energy = 100 meV. (b) Ideal case for complete charge carrier dissociation.

$$\Delta G_{CS,opt} > E_{GP} \quad (11)$$

for systems relying on a hot dissociation mechanism to generate carriers. This is in contrast to the conventional design rule $\Delta G_{CSt} \geq 0.3$ eV as suggested in early materials design studies by Scharber *et al.* and Koster *et al.*[20,21] It also suggests that achieving >10% efficiency, or moving the state-of-the-art from an efficiency landscape of Fig. 4a to that of Fig. 4b, will require more than simple energy level tuning. Importantly, these predictions are in accord with reported device efficiencies to date. A recent report by Nayak *et al.* comparing voltage losses in OPVs over that predicted by Shockley and Queisser empirically identifies this same trend.[54]

3.3 Optimal bandgap analysis

From the original solar cell efficiency limit models, including the Shockley–Queisser limit,[71] bandgaps thought to produce the highest theoretical efficiencies for inorganic single-layer solar cells have been relatively low – *i.e.*, $E_g \approx 1.1$–1.5 eV. There is also a history of success in fabricating high-efficiency solar cells from low bandgap Si ($E_g = 1.1$ eV)[72] and GaAs ($E_g = 1.43$ eV).[72]

Using the AM1.5G spectrum, Henry estimated the optimal bandgap energy to be ~1.35 eV.[73] Thus, both experimental and theoretical results for inorganic PV materials indicate that low bandgaps (~1.1 to 1.5 eV) should afford optimal efficiencies in these systems. Nevertheless, many successful OPV materials have relatively large bandgaps, in the range of $E_g = 1.7$–2.0 eV.[10] The concern with these higher E_g materials is clear: there is a sacrifice in the number of photons that can be harvested and converted to current. From simple integration of the AM1.5G spectrum, the maximum current density approximately doubles from ~15 mA cm^{-2} to ~29 mA cm^{-2} as bandgap decreases from $E_g = 2.0$ eV to $E_g = 1.5$ eV. Previous work argues from these considerations that optimal OPV bandgaps are at ~1.4 to 1.5 eV.[20]

In comparison to the traditional low-bandgap guidelines for optimal PCE, the present analysis yields notably different results. Fig. 5 shows the donor bandgap *vs.* PCE for the baseline case (*i.e.*, geminate pair binding energy = 100 meV), where the optimal bandgap = ~1.65 to 1.7 eV. This optimal magnitude is relatively large compared to inorganic solar cell results and suggests that optimum organic and inorganic solar cell energy designs rules are very different. These results also diverge from earlier OPV performance models that support optimal bandgaps of ~1.4 to 1.5 eV.[20] Note also that low bandgap materials can perform reasonably well (*e.g.*, calculated PCE = ~9% for bandgap = 1.4 eV); however, the present results also suggest that redshifting to bandgap energies below ~1.7 eV for this baseline case will in fact bring about some reduction in the optimal PCE.

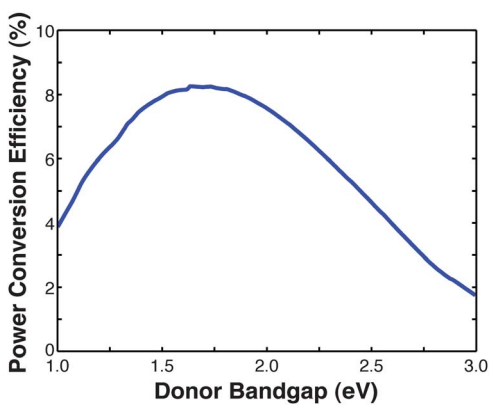

Fig. 5 Modeled optimal donor bandgap *vs.* power conversion efficiency for the baseline case (geminate pair binding energy = 100 meV).

In accord with recent OPV studies,[21,74,75] this model suggests that the reason for these differences between OPVs and their inorganic counterparts is that OPVs require an energy offset (*i.e.*, ΔG_{CS}) for effective electron–hole pair dissociation. As a result of this potential energy loss from ΔG_{CS}, the cell voltage is compromised for a given bandgap – the voltage limit is now reduced from E_g to $E_g - \Delta G_{CS}$. To counteract this loss, the bandgap must be increased. Furthermore, anticipated gains from enhanced absorption are typically mitigated by incomplete geminate dissociation[45] or competitive energy transfer[76] in low bandgap materials. Smaller bandgaps (1.1–1.5 eV) are desirable in non-excitonic cells (*e.g.*, silicon, GaAs) because these systems do not require an energy offset (ΔG_{CS}) to drive electron–hole dissociation. This observation helps explain why current state-of-the-art OPVs have sizeable 1.7–1.8 eV bandgaps, despite the extensive efforts that have been expended investigating lower bandgap alternatives. Finally, as binding energies move toward zero, the optimal bandgap shifts toward lower values. These results highlight the sensitivity of OPV power conversion efficiencies to the efficiency of the geminate pair dissociation process. As successful strategies are developed to ensure high dissociation yields at low offsets, the traditional design rules can be recovered.

4. Conclusions

The "hot dissociation" model suggested here improves considerably on traditional OB theory by moving the timescale for dissociation to be in line with experimental evidence, and provides a direct input for the energetic offset ΔG_{CS}, an important parameter for materials design. Predictions based upon this model of dissociation reproduce several trends in the literature, including the success of moderate bandgap donor polymers ($E_{g,D}$ 1.6–1.7 eV) and the reduced charge separation efficiency of low offset (ΔG_{CS}) systems.

Within the context of a hot dissociation model, further improvement could clearly be made through reduced binding energies of the CT state. Approaches to lowering the binding energy include increasing: (i) permittivity[77] and (ii) molecular π-system dimensions.[78] However, to date, these approaches have proved difficult to implement. In light of the relatively low predicted ultimate efficiencies suggested by Fig. 4a, it is undesirable for the only dissociation mechanism to be hot dissociation. Fundamentally, thermal dissociation will always require a sacrificially large ΔG_{CS} to achieve dissociation, and therefore, it is desirable to minimize this loss. In this regard, direct electronic dissociation ($S_1 \rightarrow CS$)[62] provides a way forward; as has been suggested by Muntwiler *et al.*[49] and Huang *et al.*,[79] separation of the CT state once it is formed is an energetically costly process, and microscopic design strategies should focus on avoiding the formation of this state. These recent findings suggest that observed high charge separation rates in OPVs are in part due to

efficient direct electronic dissociation rather than thermally assisted dissociation of the CT state. The very recent experimental study by Bakulin *et al.* also seems to suggest that the role of thermal dissociation can vary greatly from system to system and that direct electronic coupling to the CS state may be important for dissociation.[62] Additionally, as was recently pointed out by Faist *et al.*, achieving dissociation at low offsets must also overcome the obstacle of competitive energy transfer, which may require exploration of alternative acceptors that are not considered in this account.[76] As device efficiencies continue to rise, it must be further assessed to what extent hot dissociation is in fact the sole operant mechanism for geminate pair dissociation in these systems.

Acknowledgements

We thank the ANSER Energy Frontier Research Center funded by the Department of Energy, Grant DE-SC0001059 for support of this research. J.D.S. thanks the Link Foundation for a graduate fellowship. We thank L. Yu and Y. Liang for data from ref. 9, and H. Karmel and I. Franco for useful discussions.

Notes and references

1 C. W. Tang, *Appl. Phys. Lett.*, 1986, **48**, 183–185.
2 N. S. Sariciftci, L. Smilowitz, A. J. Heeger and F. Wudl, *Science*, 1992, **258**, 1474–1476.
3 J. J. M. Halls and R. H. Friend, *Synth. Met.*, 1997, **85**, 1307–1308.
4 G. Li, V. Shrotriya, J. Huang, Y. Yao, T. Moriarty, K. Emery and Y. Yang, *Nat. Mater.*, 2005, **4**, 864–868.
5 J. Peet, J. Y. Kim, N. E. Coates, W. L. Ma, D. Moses, A. J. Heeger and G. C. Bazan, *Nat. Mater.*, 2007, **6**, 497–500.
6 S. E. Shaheen, D. S. Ginley and G. E. Jabbour, *MRS Bull.*, 2005, **30**, 10–19.
7 H. Y. Chen, J. H. Hou, S. Q. Zhang, Y. Y. Liang, G. W. Yang, Y. Yang, L. P. Yu, Y. Wu and G. Li, *Nat. Photonics*, 2009, **3**, 649–653.
8 K. M. Coakley and M. D. McGehee, *Chem. Mater.*, 2004, **16**, 4533–4542.
9 Y. Y. Liang, Z. Xu, J. B. Xia, S. T. Tsai, Y. Wu, G. Li, C. Ray and L. P. Yu, *Adv. Mater.*, 2010, **22**, E135–E138.
10 G. Dennler, M. C. Scharber and C. J. Brabec, *Adv. Mater.*, 2009, **21**, 1323–1338.
11 B. Kippelen and J. L. Bredas, *Energy Environ. Sci.*, 2009, **2**, 251–261.
12 A. W. Hains, Z. Liang, M. A. Woodhouse and B. A. Gregg, *Chem. Rev.*, 2010, **110**, 6689–6735.
13 M. Helgesen, R. Sondergaard and F. C. Krebs, *J. Mater. Chem.*, 2010, **20**, 36–60.
14 M. A. Green, K. Emery, Y. Hishikawa and W. Warta, *Prog. Photovoltaics*, 2011, **19**, 84–92.
15 R. F. Service, *Science*, 2011, **332**, 293.
16 http://www.polyera.com/newsflash/polyera-achieves-world-record-organic-solar-cell-performance, accessed 12 April 2012.
17 http://www.osa-direct.com/osad-news/tandem-organic-photovoltaic-reaches-106-efficiency-a-worlds-first-for-polymer-organic-photovoltaic-devices.html, accessed 12 April 2012.
18 K. H. Lee, P. E. Schwenn, A. R. G. Smith, H. Cavaye, P. E. Shaw, M. James, K. B. Krueger, I. R. Gentle, P. Meredith and P. L. Burn, *Adv. Mater.*, 2011, **23**, 766–770.
19 S. H. Park, A. Roy, S. Beaupre, S. Cho, N. Coates, J. S. Moon, D. Moses, M. Leclerc, K. Lee and A. J. Heeger, *Nat. Photonics*, 2009, **3**, 297–303.
20 M. C. Scharber, D. Wuhlbacher, M. Koppe, P. Denk, C. Waldauf, A. J. Heeger and C. L. Brabec, *Adv. Mater.*, 2006, **18**, 789–794.
21 L. J. A. Koster, V. D. Mihailetchi and P. W. M. Blom, *Appl. Phys. Lett.*, 2006, **88**, 093511.
22 J. D. Servaites, M. A. Ratner and T. J. Marks, *Appl. Phys. Lett.*, 2009, **95**, 163302.
23 A. B. Tamayo, X. D. Dang, B. Walker, J. Seo, T. Kent and T. Q. Nguyen, *Appl. Phys. Lett.*, 2009, **94**, 103301.
24 X. Gong, M. Tong, F. G. Brunetti, J. Seo, Y. Sun, D. Moses, F. Wudl and A. J. Heeger, *Adv. Mater.*, 2011, **23**, 2272–2277.
25 K. Vandewal, K. Tvingstedt, A. Gadisa, O. Inganäs and J. V. Manca, *Nat. Mater.*, 2009, **8**, 904–909.
26 R. B. Ross, C. M. Cardona, D. M. Guldi, S. G. Sankaranarayanan, M. O. Reese, N. Kopidakis, J. Peet, B. Walker, G. C. Bazan, E. Van Keuren, B. C. Holloway and M. Drees, *Nat. Mater.*, 2009, **8**, 208–212.
27 L. Onsager, *J. Chem. Phys.*, 1934, **2**, 599–615.
28 C. L. Braun, *J. Chem. Phys.*, 1984, **80**, 4157–4161.
29 V. D. Mihailetchi, L. J. A. Koster, J. C. Hummelen and P. W. M. Blom, *Phys. Rev. Lett.*, 2004, **93**, 216601.
30 N. C. Giebink, G. P. Wiederrecht, M. R. Wasielewski and S. R. Forrest, *Phys. Rev. B: Condens. Matter Mater. Phys.*, 2010, **82**, 155305.
31 P. Peumans and S. R. Forrest, *Chem. Phys. Lett.*, 2004, **398**, 27–31.
32 T. Offermans, S. Meskers and R. Janssen, *Chem. Phys.*, 2005, **308**, 125–133.
33 M. M. Mandoc, W. Veurman, L. J. A. Koster, B. de Boer and P. W. M. Blom, *Adv. Funct. Mater.*, 2007, **17**, 2167–2173.
34 D. Veldman, O. İpek, S. C. J. Meskers, J. Sweelssen, M. M. Koetse, S. C. Veenstra, J. M. Kroon, S. S. van Bavel, J. Loos and R. A. J. Janssen, *J. Am. Chem. Soc.*, 2008, **130**, 7721–7735.
35 C. Deibel, T. Strobel and V. Dyakonov, *Phys. Rev. Lett.*, 2009, **103**, 036402.
36 I. A. Howard, R. Mauer, M. Meister and F. Laquai, *J. Am. Chem. Soc.*, 2010, **132**, 14866–14876.
37 M. L. Zhang, H. Wang and C. W. Tang, *Appl. Phys. Lett.*, 2010, **97**, 143503.
38 J. L. Brédas, J. E. Norton, J. Cornil and V. Coropceanu, *Acc. Chem. Res.*, 2009, **42**, 1691–1699.
39 C. Dyer-Smith, L. X. Reynolds, A. Bruno, D. D. C. Bradley, S. A. Haque and J. Nelson, *Adv. Funct. Mater.*, 2010, **20**, 2701–2708.
40 S. Difley, D. Beljonne and T. Van Voorhis, *J. Am. Chem. Soc.*, 2008, **130**, 3420–3427.
41 R. Pensack and J. Asbury, *J. Am. Chem. Soc.*, 2009, **131**, 15986–15987.
42 R. D. Pensack and J. B. Asbury, *J. Phys. Chem. Lett.*, 2010, **1**, 2255–2263.
43 J. Lee, K. Vandewal, S. R. Yost, M. E. Bahlke, L. Goris, M. A. Baldo, J. V. Manca and T. Van Voorhis, *J. Am. Chem. Soc.*, 2010, **132**, 11878–11880.
44 T. Drori, C.-X. Sheng, A. Ndobe, S. Singh, J. Holt and Z. Vardeny, *Phys. Rev. Lett.*, 2008, **101**, 037401.
45 H. Ohkita, S. Cook, Y. Astuti, W. Duffy, S. Tierney, W. Zhang, M. Heeney, I. McCulloch, J. Nelson, D. D. C. Bradley and J. R. Durrant, *J. Am. Chem. Soc.*, 2008, **130**, 3030–3042.
46 V. I. Arkhipov, E. V. Emelianova and H. Bässler, *Phys. Rev. Lett.*, 1999, **82**, 1321.
47 T. M. Clarke, A. M. Ballantyne, J. Nelson, D. D. C. Bradley and J. R. Durrant, *Adv. Funct. Mater.*, 2008, **18**, 4029–4035.
48 A. C. Morteani, P. Sreearunothai, L. M. Herz, R. H. Friend and C. Silva, *Phys. Rev. Lett.*, 2004, **92**, 247402.
49 M. Muntwiler, Q. Yang, W. A. Tisdale and X. Y. Zhu, *Phys. Rev. Lett.*, 2008, **101**, 196403.
50 F. Etzold, I. Howard, R. Mauer, M. Meister, T.-D. Kim, K.-S. Lee, N. S. Baek and F. Laquai, *J. Am. Chem. Soc.*, 2011, **133**, 9469–9479.
51 X. Y. Zhu and A. Kahn, *MRS Bull.*, 2010, **35**, 443–448.
52 J. J. Benson-Smith, L. Goris, K. Vandewal, K. Haenen, J. V. Manca, D. Vanderzande, D. D. C. Bradley and J. Nelson, *Adv. Funct. Mater.*, 2007, **17**, 451–457.
53 T. M. Clarke and J. R. Durrant, *Chem. Rev.*, 2010, **110**, 6736–6767.
54 P. K. Nayak, J. Bisquert and D. Cahen, *Adv. Mater.*, 2011, **23**, 2870–2876.
55 J. J. M. Halls, J. Cornil, D. A. dos Santos, R. Silbey, D. H. Hwang, A. B. Holmes, J. L. Bredas and R. H. Friend, *Phys. Rev. B: Condens. Matter Mater. Phys.*, 1999, **60**, 5721–5727.
56 D. R. Anderson, *Chem. Rev.*, 1966, **66**, 677–690.
57 J. Huang and R. B. Kaner, *Nat. Mater.*, 2004, **3**, 783–786.
58 V. I. Arkhipov, E. V. Emelianova, S. Barth and H. Bässler, *Phys. Rev. B: Condens. Matter Mater. Phys.*, 2000, **61**, 8207.
59 M. Hallermann, S. Haneder and E. D. Como, *Appl. Phys. Lett.*, 2008, **93**, 053307.
60 B. Walker, A. B. Tamayo, X.-D. Dang, P. Zalar, J. H. Seo, A. Garcia, M. Tantiwiwat and T.-Q. Nguyen, *Adv. Funct. Mater.*, 2009, **19**, 3063–3069.

61 C. M. Cardona, W. Li, A. E. Kaifer, D. Stockdale and G. C. Bazan, *Adv. Mater.*, 2011, **23**, 2367–2371.
62 A. A. Bakulin, A. Rao, V. G. Pavelyev, P. H. M. van Loosdrecht, M. S. Pshenichnikov, D. Niedzialek, J. r. m. Cornil, D. Beljonne and R. H. Friend, *Science*, 2012, **335**, 1340–1344.
63 W. Shockley, *T Tech. J.*, 1949, **28**, 435–489.
64 W. J. Potscavage, S. Yoo and B. Kippelen, *Appl. Phys. Lett.*, 2008, **93**, 193308.
65 G. Li, V. Shrotriya, J. S. Huang, Y. Yao, T. Moriarty, K. Emery and Y. Yang, *Nat. Mater.*, 2005, **4**, 864–868.
66 L. J. A. Koster, M. Kemerink, M. M. Wienk, K. Maturová and R. A. J. Janssen, *Adv. Mater.*, 2011, **23**, 1670–1674.
67 D. Veldman, S. C. J. Meskers and R. A. J. Janssen, *Adv. Funct. Mater.*, 2009, **19**, 1939–1948.
68 D. Credgington, R. Hamilton, P. Atienzar, J. Nelson and J. R. Durrant, *Adv. Funct. Mater.*, 2011, **21**, 2744–2753.
69 J. M. Szarko, J. Guo, Y. Liang, B. Lee, B. S. Rolczynski, J. Strzalka, T. Xu, S. Loser, T. J. Marks, L. Yu and L. X. Chen, *Adv. Mater.*, 2010, **22**, 5468–5472.
70 W. L. Ma, C. Y. Yang, X. Gong, K. Lee and A. J. Heeger, *Adv. Funct. Mater.*, 2005, **15**, 1617–1622.
71 W. Shockley and H. J. Queisser, *J. Appl. Phys.*, 1961, **32**, 510–519.
72 B. G. Streetman and S. Banerjee, *Solid State Electronic Devices*, Prentice Hall, 2000.
73 C. H. Henry, *J. Appl. Phys.*, 1980, **51**, 4494–4500.
74 T. Kirchartz, K. Taretto and U. Rau, *J. Phys. Chem. C*, 2009, **113**, 17958–17966.
75 D. Godovsky, *Org. Electron.*, 2011, **12**, 190–194.
76 M. A. Faist, T. Kirchartz, W. Gong, R. S. Ashraf, I. McCulloch, J. C. de Mello, N. J. Ekins-Daukes, D. D. C. Bradley and J. Nelson, *J. Am. Chem. Soc.*, 2012, **134**, 685–692.
77 R. Kroon, M. Lenes, J. C. Hummelen, P. W. M. Blom and B. De Boer, *Polym. Rev.*, 2008, **48**, 531–582.
78 K. Hummer and C. Ambrosch-Draxl, *Phys. Rev. B: Condens. Matter Mater. Phys.*, 2005, **71**, 081202.
79 Y.-S. Huang, S. Westenhoff, I. Avilov, P. Sreearunothai, J. M. Hodgkiss, C. Deleener, R. H. Friend and D. Beljonne, *Nat. Mater.*, 2008, **7**, 483–489.

